

# Gradient-based kernel selection technique for tumour detection and extraction of medical images using graph cut

ISSN 1751-9659  
 Received on 9th December 2018  
 Revised 21st March 2019  
 Accepted on 14th October 2019  
 E-First on 28th November 2019  
 doi: 10.1049/iet-ipr.2018.6615  
 www.ietdl.org

Jyotsna Dogra<sup>1</sup> ✉, Shruti Jain<sup>1</sup>, Meenakshi Sood<sup>1\*</sup>

<sup>1</sup>Department of Electronics and Communication, Jaypee University of Information Technology, Wakhnaghat, Solan, India

\*Current affiliation: National Institute of Technical Teachers Training & Research, Chandigarh, MHRD, India

✉ E-mail: jyotsnadogra1989@gmail.com

**Abstract:** Magnetic resonance imaging is a powerful, ubiquitous imaging technique that provides detailed high-contrast images differentiating soft tissues. The low radio-frequency bias field creates intensity inhomogeneity generating low contrast that often creates difficulty for quantitative and qualitative analyses. Segmentation aids in analysis of changes occurring in brain, where bias effect severely affects performance. The graph-cut (GC) segmentation provides supervised computer-assisted diagnosis and treatment. GC's interactive nature requires manual selection of kernels for initialisation. The shrinkage behaviour of GC creates inaccurate and fallacious extraction. On the basis of these problems, this study proposes gradient-based kernel selection GC method that simultaneously removes shrinkage problem and locates tumour in image, eliminating human interaction with accurate segmentation for even bias field images. The proposed method addresses these problems by emphasising on directive inclination of intensity scales of symmetrical halves of images. The proposed method is evaluated for high-grade glioma and low-grade glioma images with and without bias field. The average performance metrics evaluated for these images depict remarkable improvement in comparison with existing techniques. The proposed technique is validated by applying on real-time dataset of tumour images obtained from State Government Hospital, Shimla, India.

## 1 Introduction

Magnetic resonance imaging (MRI) is the standard technique used for brain tumour diagnosis. This technique is widely used in clinics as it provides a different type of tissue contrast by varying the excitation and repetition times [1]. The analysis and study of brain tumour MRI images are considered to be complex and challenging. This is due to the tumour's heterogeneous structure that generates difficulty in locating the boundary. Also, tumour growth and formation are integrally unpredictable.

Consequently, the shape and different textural properties do not fall into a standard set of shape or size. Besides these difficulties, a bias field effect corrupts MR images by creating the intensity inhomogeneity [2]. Bias field is a low-frequency undesirable signal that has varying intensity distribution with multiplicative nature. These invariabilities are biggest hurdle in medical analysis. The intensity inhomogeneity is particularly severe in MRI at ultra-high field strengths (e.g. 3 and 7 T) and sometimes makes it difficult even for expert human observers to view the images.

To provide an efficient and impartial evaluation medical image analysis is gaining attention. With the huge on-going research in this field, many methods reported are closer to the routine clinical application. One of the methods in image analysis is segmentation technique that allows the extraction of the abnormal tissue from the normal. This extraction is helpful for the feature and texture analyses of the tumour. There has been an enormous work in the field of image segmentation. Among various segmentation techniques, the automatic image segmentation is an active area of research work, which has attracted significant attention. To fully automate the method, user interaction must be completely terminated. The accurate knowledge of prior information is critical and depends on the preferences of the segmented region for the ultimate goal of segmentation. Owing to the intensity dependence of the selection of these a priori information from the images with bias effect becomes much difficult.

One of the popularly used segmentation technique in image analysis is the graph-cut (GC) method [3]. The energy function used in this method consists spatial coherency term and data term. The former term evaluates the abrupt changes in the boundary. The

latter is the likelihood energy that defines the Gaussian intensity distribution of the MR brain image. This distribution is formed if the kernel value obtained from the selected markers, indicating the highest resemblance with the object and the background region, are known (which are the prior information). The kernels are key values that are used to localise the tumour in the brain MR image and initialise the subsequent steps of the segmentation process. The domain priors can be empirically or randomly selected [4] with the help of radiologist for the breast tumour. Researchers have also initialised the algorithm with random pixel values and detected the texture feature and spatial characteristics of the object region for automating the segmentation method [5, 6].

### 1.1 Our contribution

With the variant application-driven advantages provided by the GC method, on the one hand, it partakes the limitation of small cuts or shrinkage behaviour [7, 8]. There is an occurrence of the erroneous pixel regions, which mainly occur due to more than one tumour settlements comprising high affinity with the tumour region. In this work, the focus is on estimating the kernels that serve important purposes of segmentation for all images, with and without bias field. The proposed gradient-based kernel selection GC (GBKS GC) technique focuses on the abrupt changes caused due to the glioma-affected areas. These abrupt changes are evaluated, and pixel location forms the initial markers providing the essential kernel values. It eliminates user interaction and creates a fully automatic algorithm. The selection of accurate kernels aids in obtaining single-connected region and removal of shrinkage problem. On applying the proposed method on MR images affected by the bias field, accurate segmentation of the tumour region achieved. Moreover, the proposed technique gave accurate segmentation results when applied on the real-time images of the brain obtained from Government Hospital, Indra Gandhi Medical Hospital (IGMC), Shimla, Himachal Pradesh (India). The brief description of the achieved objectives is discussed below:

- *Automatic marker selection for the GC algorithm:* The GC algorithm depends on the intensity values of the brain image and

requires markers for its initialisation. In this paper, we have provided the kernel values by using the pixel intensity and exploiting the symmetrical nature of brain structure. Also, the selection of markers is done without any human intervention achieving automatic initialisation.

- *Removing shrinkage problem:* To detect a complete tumour region excluding any extra or erroneous region, the kernel values are extracted with their site of the existence to eliminate these regions. By including these sites during segmentation, an effective extraction of the homogeneous single-connected region is achieved. This results in the removal of the shrinkage problem caused in the conventional GC method.
- *Removing effect of bias field:* The bias field creates abrupt intensity changes that may affect the marker selection and consequently the segmentation. The segmented tumour region contains abrupt boundaries and the inherent intensity inhomogeneity causes due to the bias field inside the object region. This abruptness and non-uniformity in the segmented tumour are removed by applying the proposed GBKS GC technique.

## 1.2 Related work

Among the various interactive methods, GC segmentation employs Gaussian mixture models (GMMs) for intensity distribution, and its energy equation formulates the cut for partitioning the foreground [9]. The GrabCut uses an iterative energy minimisation by utilising two GMMs providing intensity distribution for both the object and foreground regions [10]. Owing to its interactive nature, a bounding box is required, drawn by the user that encloses the object. The intelligent scissor technique [11] uses the user-defined points and crops the nearest object region boundary. The extraction is done via graph search methods for its automatic execution. In this research work, automatic GC segmentation is employed by removing this interactive nature and providing the most accurate markers to perform good object segmentation.

Even if the interactive nature of this technique is removed still some unwanted region is segmented along the object region due to the shrinkage bias. These are formed for the region with the shorter boundary as there are intensity discontinuities at the boundary of the segmented region. This problem presents a difficulty for segmenting a single-connected object region. The normal brain MR image region is disguised as the infected tumour region. To address this, issues of some methods are reported to remove this problem. Jermyn and Ishikawa [12], Sinop and Grady [13], Kimmel and Bruckstein [14] and Kolmogorov and Boykov [15] demonstrated a flux of a vector field to overcome the shrinkage problem. Mostly this technique is applied on thin objects, for example, blood vessel grey-scale image of the human body. In these images, the object and background regions are represented by intensity values varying from white till grey. The vector fields are created by observing the image gradients. However, these methods lack two major aspects: first, this approach does not work on the colour image, and second, it faces the issue of choosing the initial vector field. In GC technique, Boykov *et al.* [16] demonstrated an approximate solution for multiple labelling. The terminal and non-terminal links obtained from the normalised cuts described by Shi and Malik [17] partitions the graph forming the disconnected and connected avoids the problem. Hao *et al.* [18], Gao *et al.* [19], Alemán-Flores *et al.* [20] and Liu *et al.* [21] applied this approach for segmenting lesions in the breast ultrasound images. A necessary requirement of the initial markers is critical for the initialisation of an automatic algorithm. These initial markers are given by Hanaoka *et al.* [3] by proposing a Riemannian metric for the three-dimensional (3D) image by enhancing the GC segmentation and consequently solving the shrinking problem. This Riemannian metric provides prior knowledge of the predefined shape or initial contour. However, this method remains limited while segmenting the thin-elongated object.

Besides, the different approaches discussed above for segmentation, a major issue also lies in partitioning the tumour from a bias field affected image. To reduce this effect many researchers have reported literature on the removal of the bias

effect on MR images [22, 23]. Sled *et al.* [22] proposed an iterative and automatic non-parametric non-uniform intensity normalisation ( $N3$ ) approach, in which no a priori information was used. Wells *et al.* [23] presented an adaptive estimation method by employing expectation maximisation. This method is able to segment each brain tissue, but accurate knowledge of a priori information is required. Li *et al.* [24] used the coherent local intensity clustering for estimating the bias field and segmenting the object region. Image denoising is done by Bilenia *et al.* [25] for removing the bias field from the T1 modality of the brain MRI images with skull stripping at the initial phase.

Many researchers introduce many semi-automatic and automatic approaches regarding GC technique are in the past few years. In semi-automatic approach, some of the clustering techniques are developed by researchers [26–28]. The region growing method is combined with two clustering method:  $k$ -mean and fuzzy  $c$ -mean (FCM) to provide a multi-stage approach [26]. This technique aided in segmented following regions: peritumoural region and enhancing tumour region. Also, a multidimensional feature set is constructed that comprise texture characteristics of different MRI modalities (T1, T1ce and T2) [27]. The  $k$ -mean clustering method is used on these feature sets and a Dirichlet a priori segmentation is easily performed as normal brain region intensity clusters are completely omitted from the feature set framed. Another hybrid technique for multi-stage segmentation Kanas *et al.* [28] used random walks and FCM approach.

Jiang *et al.* [29] proposed a semi-automatic approach that included training through learning with the help of some feature sets. This method is applied on all the modalities (i.e. T1, T1ce, T2 and flair). In this approach, classifier is trained through learning by providing the population feature sets. The segmentation is performed using a GC technique considering the probability maps formed by the classifiers. Zhao *et al.* [30] used Markov random field for extraction with good accuracy. This proposed method is applied to the complete set of modalities, except for T1. The technique presented by Ilunga-Mbuyamba *et al.* [31] employs a hybrid form of active contour model and  $k$ -mean. This technique of using active contour model enhances the speed for the process of segmentation.

Mostly, the fully automatic approaches use the neural network as it extracts high-level information from the dataset to provide the learning. These methods are highly accurate and fully automatic requiring a large amount of data for the learning process. The neural network approaches developed by the researchers [32–35] collect the key prior information required for the segmentation. Havaei *et al.* [32] presented a deep neural network that uses global and local contextual features. This network comprises training at a two-phase level to remove any imbalance that occurs in the tumour labels. A toolkit named ilastik is also used for extraction [33] that does not employ any human interaction. Zikic *et al.* [34] applied convolutional neural network with all likelihood to directly apply segmentation to the brain tumour tissues. The labelling to all the surrounding tissue is provided with respect to the information generated by the network. A classification within the tumour region is also done by Havaei *et al.* [35] by employing a neural network. Li *et al.* [36] have provided a likelihood estimation using a machine learning method that gave the best estimation and good accuracy value for the segmentation using GCs. Wu and Yizhou [37] proposed an automatic method for fine quality extraction of objects from photographs. The foreground pixels are extracted to form texture feature using classifiers and convolution features are generated using a deep neural network. These feature aids in the extraction of the objects.

This paper is organised in the following sections: Section 2 contains the problem formulation. Section 3 comprises the materials and methodology. In Section 4, the experimental results obtained are tabulated and the output images obtained are depicted. Also, a comparison of our result with the existing method is tabulated in this section. Finally, in Section 5, the conclusion and future work are formulated.

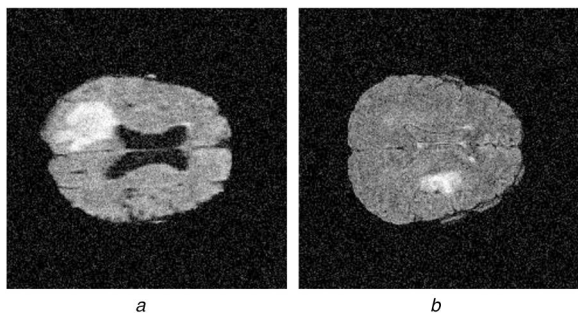


**Fig. 1** Bias field MR images  
(a) HGG, (b) LGG

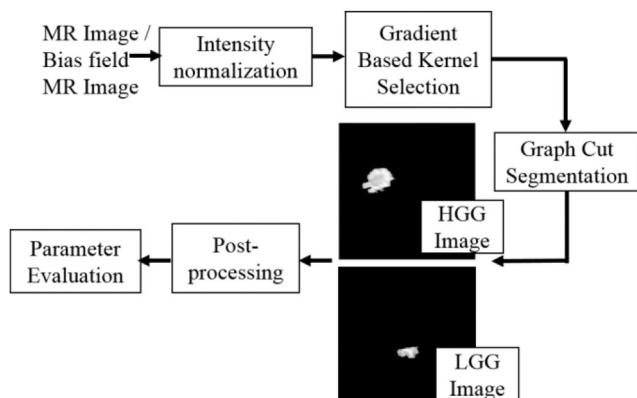


**Fig. 2** Proposed GBKS GC segmentation technique

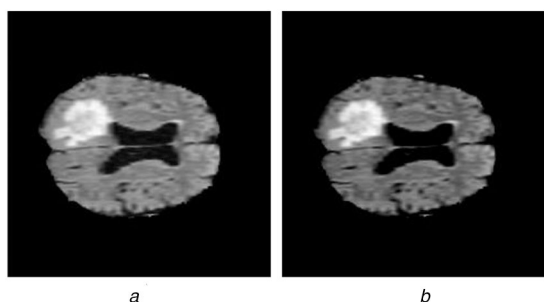


**Fig. 3** Effect of intensity normalisation on one of the flair image  
(a) Original MR flair image, (b) Intensity normalised image

## 2 Problem formulation

The general structure of graph  $G = \langle \nu, \epsilon \rangle$  consists of  $\nu$  nodes which represents the pixels and  $\epsilon$  edges formed by the neighbouring pixels. For bi-object segmentation, the source  $s$  and sink terminals  $t$  are required for partitioning the graph in the object and the background region. The connectedness of these terminals with the graph is shown by an arc known as ' $t$ -link' (terminal link). The second type of arc is the ' $n$ -link' (non-terminal link), which connects the neighbouring pixels. The  $s/t$  cut in the graph is a partitioning of  $\nu$  into two disjoint sets of  $s$  and  $t$ . A cut with minimal cost is the best cut applied. This cut is obtained by minimising the energy function. The energy equation comprises of the summation of data and spatial coherency term. The standard energy function for GC-based image segmentation approaches [9, 10] in the equation below:

$$E(x) = \sum_{p \in \nu} E_p(x_p) + \sum_{(p, q) \in \epsilon} E_{pq}(x_p, x_q) \quad (1)$$

Our goal is to obtain kernels for the initialisation of the algorithm without any user interaction and remove the shrinkage problem in the GC method. These goals are obtained under certain connectivity constraints. These constrained assume that an undirected graph with defined connectivity between the nodes is

provided. In our experiment, a 2D grid graph with energy equation given in (1) is considered.

To perform segmentation, complete image must be partitioned as:  $x \in \{x_O, x_B\}$ , where  $x_O$  and  $x_B$  are the sets of pixels belonging to the object and background region, respectively. These sets associate high resemblance with the selected kernel ( $s$  and  $t$ ) that even aids in the initialisation of the GC methodology. The path formed between  $s$  and  $t$  must consist of connected nodes  $x_O$ . One way for the marker selection is to provide a user interface by clicking on image. These markers help in creating the kernels. Unfortunately, this user interaction employs multiple clicks and it becomes a non-deterministic polynomial hard problem. Once the segmentation is performed, it is difficult to obtain a single-connected component due to problem of shrinkage. As the object pixel set is labelled as 1,  $x_O = \{x_O \in x | x_O = 1\}$  and the small area formed due to small cuts, the extra regions are obtained. In an interactive environment, it is possible that inaccurate prior information is considered and structures are incorrectly segmented. Even the bias field MR images that portray non-uniformity of the intensity scale creates even bigger challenge for selecting the markers. This intensity inhomogeneity in the MR images can be observed from Fig. 1.

## 3 Material and methodology

The dataset for conducting the experiment for this research work are taken from the Brain Tumour Segmentation Challenge, a part of MICCAI challenges [38–40]. This dataset consists of different types of glioma images comprising high-grade glioma (HGG) and low-grade glioma (LGG). There are four modalities of size  $240 \times 240$  which are co-registered and low-intensity tumour images [41], namely T1, T1ce, T2 and flair. For our research work, 70 and 70 LGG flair images without any bias field effect and with bias field effect are utilised and the evaluated results are reported. To validate the experimental results, the ground truth (GT) provided by the expert radiologists is used.

The real-time dataset comprising meningioma and glioblastoma multiforme (GBM) MR images are obtained from the radiology department of State Government Hospital, IGMC, Shimla, Himachal Pradesh (India).

The proposed method consists of five main steps: intensity normalisation, marker selection, GC segmentation, post-processing and parameter evaluation. The proposed technique using GBKS GC is depicted in Fig. 2.

The steps involved in the proposed algorithm are detailed in the following section.

### 3.1 Intensity normalisation

The brain MR images have intensity values in the range 0–255  $\times$  255, leading to bad estimates of mean/variance and increases the memory space. The obtained dataset provides MR image of size  $240 \times 240$  containing pixel value ranging from 0 to 65,025. By applying intensity normalisation, the size of image is reduced from 16 to 8 bit and the intensity range is converted to a scale of 0–255. Fig. 3 illustrates the effect of intensity normalisation on one of the flair image.

### 3.2 Proposed GBKS

The pictorial illustration of the proposed GBKS methodology is depicted in Fig. 4. The process is entirely intensity dependent, less iterative with low mathematical complexity. It principally depends on the gradient calculation and inclination of these gradients. Both the positive and negative inclinations represent the abrupt changes in two halves of the images.

Fig. 4 depicts a two-level division of the input MR image, and the extraction of the markers with their location after converting the grey image into a binary form. The workflow of the proposed GBKS technique for marker selection is provided in Fig. 5. The pixel values in the main image  $\mathcal{I}$  and both horizontal half ( $\mathcal{I}_{1/2}^{-1}$  and  $\mathcal{I}_{1/2}$ ) of the image are used to calculate the gradient. Among these images, the inverse represents tumour region. Initially,

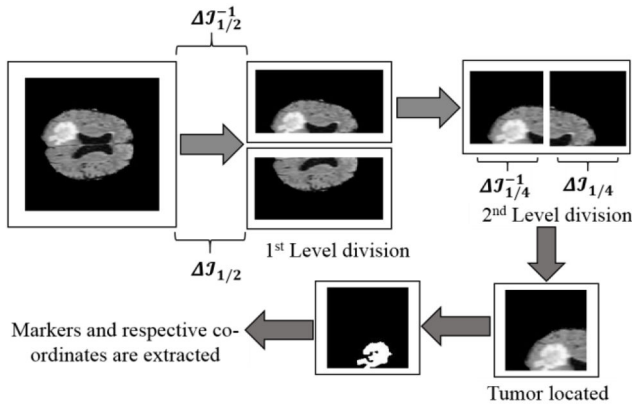


**Fig. 4** Workflow of the proposed GBKS technique

random weights are assigned to each image and the gradients are calculated. These gradients help in obtaining the majorly affected tumour region of the brain. In a normal brain image, symmetrical intensity distribution is present and the gradients do not show any inclination (negative or positive)

$$\Delta \mathcal{J}_{1/2} = \Delta(\mu_K \sim \mu_{I_{11K}}) \cong 0 \quad (2)$$

$$\Delta \mathcal{J}_{1/2}^{-1} = \Delta(\mu_K \sim \mu_{I_{12K}}) \cong 0 \quad (3)$$

At both the levels, gradients and the amount of negative slope are calculated

$$\text{amount(NS)} = \begin{cases} \sum(\text{negative}(\Delta \mathcal{J}_{1/2})) \\ \sum(\text{negative}(\Delta \mathcal{J}_{1/2}^{-1})) \end{cases} \quad (4)$$

where NS is the negative inclination.

Large amount of NS implies the presence of the tumour region in one of the horizontal half of the MR image, which is generated for the second level. The gradients and their inclination are again calculated at this level

$$I^{L2} = \begin{cases} NS > NS^{-1} \rightarrow I_{12}: \{I_{12}, I_{12}^{-1}\} \rightarrow \text{tumor presence in } I_{12} \\ NS < NS^{-1} \rightarrow I_{11}: \{I_{11}, I_{11}^{-1}\} \rightarrow \text{tumor presence in } I_{11} \end{cases} \quad (5)$$

where  $I^{L2}$  image generated for the second level of the algorithm. No further division is done after image size  $\geq (m/4) \times (n/4)$ .

After the second-level division, final image with size  $(m/4) \times (n/4)$  is converted into binary form and location of tumour and markers are calculated. These two important key points aid in the automatic initialisation and in obtaining single-connected region by removing the shrinkage problem.

The kernels that are calculated using the detected markers and their location provide an accurate tumour segmentation. The GBKS terminates any manual or interactive kernel selection, removing the inaccuracy and false segmentation. Even the problem of shrinkage is removed. The proposed method not only provides the markers, but also their location hence providing a single-connected object region. Different techniques are employed before for the selection of these kernels. Rosenfled and Pfaltz [42] segmented the image using distance transform operator that is viable for only single local maxima in target regions. Distance transform along with global thresholding is able to distinguish various regions. Park *et al.* [43] provided ultimate erosion for convex sets that is an iterative morphological algorithm required to extract the seed points from overlapping regions limited to the nanoparticles and their morphological analysis.

### 3.3 GC segmentation

The object and background kernels are evaluated from the markers obtained from the proposed GBKS method. These kernel values execute the segmentation of the tumour region by an algorithm

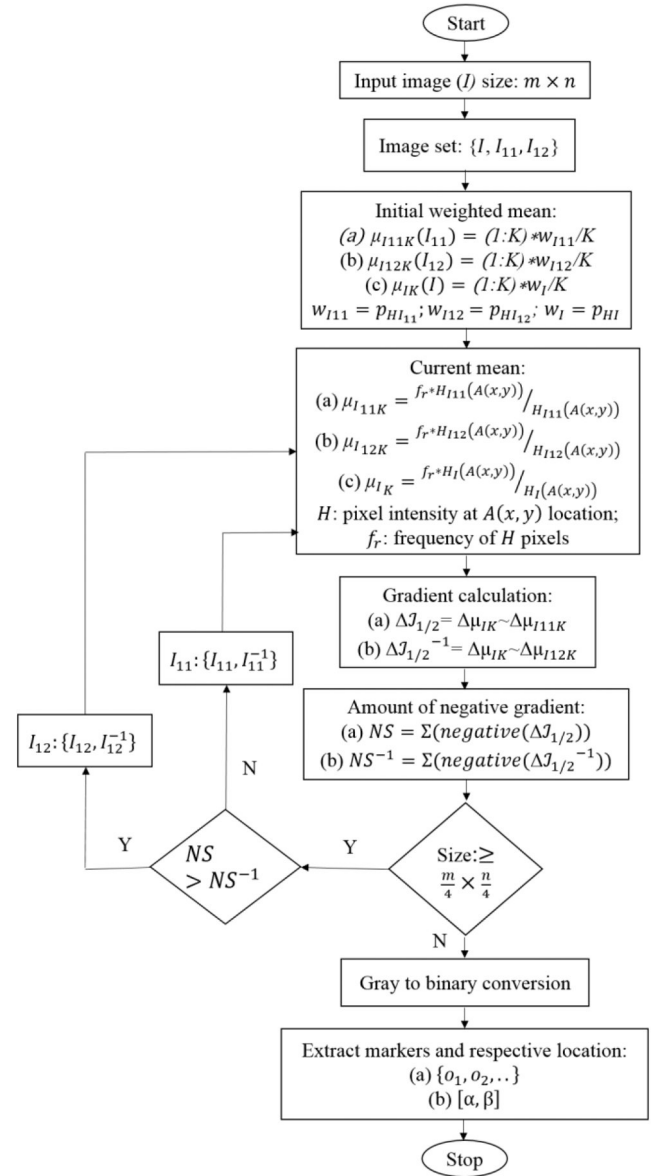


**Fig. 5** Flowchart of the proposed GBKS technique

developed by authors Dogra *et al.* [44]. Even after segmentation, the obtained image may contain some erroneous regions that occur due to the limitation of the GC method known as shrinkage problem.

The location obtained from the flowchart given in Fig. 5 create a single-connected tumour region. These location are further used for removing the shrinkage problem by the following stepwise procedure explained in Algorithm 1 (Fig. 6). All the pixels showing high similarity with these location form a single-connected tumour region resulting in the extraction of the segmented output.

### 3.4 Post-processing: bias field correction

Bias field is a multiplicative noise causing intensity inhomogeneity

$$p_i = p_i b_i; \quad i = 1, 2, 3, \dots, m \times n \quad (6)$$

where  $p_i$  is the pixel intensity at the  $i$ th position of the 2D image and  $b_i$  is the intensity variation of the bias field. This bias field has Gaussian distribution

$$b_{\text{Gauss}}(p) = \frac{1}{\sigma \sqrt{2\pi}} \exp\left(-\frac{(p - \mu)^2}{2\sigma^2}\right) \quad (7)$$

where  $p$ ,  $\sigma$  and  $\mu$  are the image intensity, standard deviation and mean value, respectively.

The performance of segmentation method on bias field images gets degraded due to intensity inhomogeneity. Therefore, removal of this bias field from the segmented images is achieved by applying post-processing technique using non-linear median filter. Fig. 7 depicts the removal of the bias field while preserving the edges of extracted region.

### 3.5 Parameter evaluation

The complete evaluation for the proposed GBKS GC is done on the basis of various parameters as reported in the literature review. Parameters calculated for the accuracy of the selected kernel are: mean square error (MSE) and correlation coefficient (CC). The MSE value quantifies the difference between the mask obtained and the GT. The strength between the variables and relationships is calculated by the CC parameter. For the validation of mask area, perimeter, major axis length (MAL) and minor axis length (MiAL) parameters of the obtained tumour region with the GT are measured. These properties give the confirmation of the shape of the obtained tumour region. To evaluate the performance of the proposed GBKS method, Jaccard index (JI), dice similarity coefficient (DSC), positive predictive value (PPV), sensitivity and specificity are calculated. The performance metrics are calculated using the parameters: true positive (TP), false positive, true negative and false negative (FN).

*DSC*: It measures the overlap or the amount of similarity in the pixel between the GT and the affected region obtained after automatic segmentation

$$DSC = \frac{2(ET \cap GT)}{(ET \cap GT) + 2(ET \cap GT) + (ET \cap GT)} \quad (8)$$

where ET is the extracted tumour and GT is the ground truth available.

*Sensitivity*: This parameter measures the number of TP and FN detections, which means it calculates the fraction of positives that are correctly detected by the experiment.

*JJ*: It is the measured amount of similarity between the two samples obtained from the GT and the segmented result

$$JI = \frac{ET \cap GT}{ET \cap GT} \quad (9)$$

*Specificity*: This parameter calculates the fraction of negatives that are correctly detected. It covers all those pixels that were not detected and the experiments does not detect them.

*PPV*: It predicts the amount of segmented region that are oversegmented or the pixel region that gets segmented even though it is the part of the normal brain tissue region.

## 4 Results and discussion

This research work addresses three major issues of automatic extraction of glioma-affected portion from MR images. The first section evaluates the effectiveness of the selected kernels in removing the shrinkage problem [7, 8]. The results are quantitatively and qualitatively validated by extracting the portion affected with bias field.

### 4.1 Automated segmentation

The proposed GBKS GC method focuses on the issues of kernel selection for the initialisation of the algorithm and removal of the shrinkage problem [7, 8].

Owing to intensity-based nature of the GC method, it is difficult to obtain a single extracted region. Small cuts and leakages are formed due to similar intensity regions in the normal part of the brain. These extra regions get extracted by the GC method, which is a limitation of this method. Figs. 8b and e show the results obtained from conventional GC for HGG and LGG brain tumour MRIs clearly indicating the fallacious segmentation regions.

**Input:** Marker co-ordinates.

**Output:** Single connected tumor region.

**Begin**

Step 1: Segmented Image:

$$L_k = \begin{cases} 0 & \text{Non-tumor region} \\ 1 & \text{Tumor Region} \end{cases}$$

Step 2: Find the neighborhood pairs  $(N_{T_\alpha}, N_{T_\beta})$  from the stored locations  $[\alpha, \beta]$

Step 3: Calculate similarity.

$$S = \text{USim}(N_{T_\alpha}, N_{T_\beta});$$

Step 4: Using property of similarity calculate similar pixels:

$$N = \{(N_{T_\alpha}, N_{T_\beta}) : s(N_{T_\alpha}, N_{T_\beta}) = \max(S)\};$$

Step 5: Obtain the single connected region

$$R_{\text{conn}} = \{N_{T_\alpha} \cup N_{T_\beta}\};$$

**End**

**Fig. 6** Algorithm 1: algorithm for extraction of single-connected tumour region using the proposed GBKS GC technique

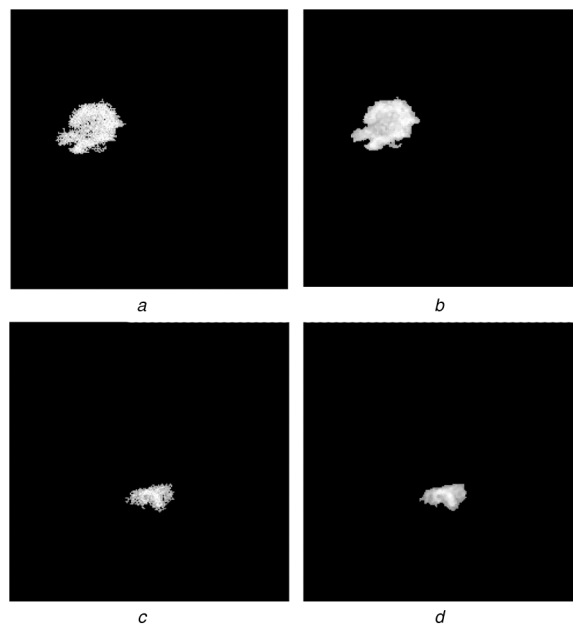


**Fig. 7** Removal of the bias field

(a), (b) Segmented bias field HGG image by the proposed algorithm and post-processing. (c), (d) Segmented bias field LGG image by the proposed algorithm and post-processing

Figs. 9b and e show the similar results for bias field MR images. For Figs. 8c and f, it is observed that by employing the proposed GBKS GC method, the shrinkage problem is completely removed as erroneous pixels are not obtained. Also, a single-connected component is obtained at the output implying accuracy in the selected kernels that initialise the algorithm. Similarly, accurate outputs are also obtained for bias field images as shown in Figs. 9c and f.

To prove the effectiveness of the proposed method in removing the shrinkage problem, MSE and CC values are obtained. The results for 20 HGG and 20 LGG MR images are illustrated in Table 1. The results reported are of GBKS GC method applied on images with and without bias field effect for both the HGG and LGG MRI images.

The average mean obtained for all 35 HGG and LGG MR images for bias field and without bias field is tabulated in Table 2. For the proposed technique, it is observed from Table 2 that the average MSE value is very low as all the extra pixels are removed. The CC value obtained by the proposed technique is higher in

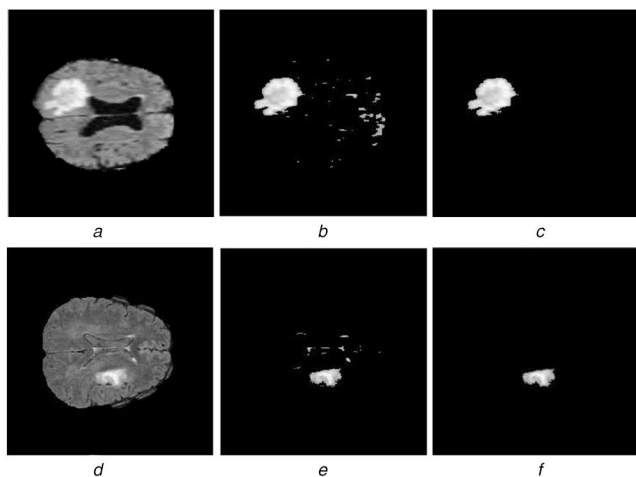


**Fig. 8** Automated segmentation  
(a), (d) Original HGG and LGG MR images, (b), (e) Segmentation showing shrinkage problem, (c), (f) Removal of shrinkage by the proposed GBKS GC

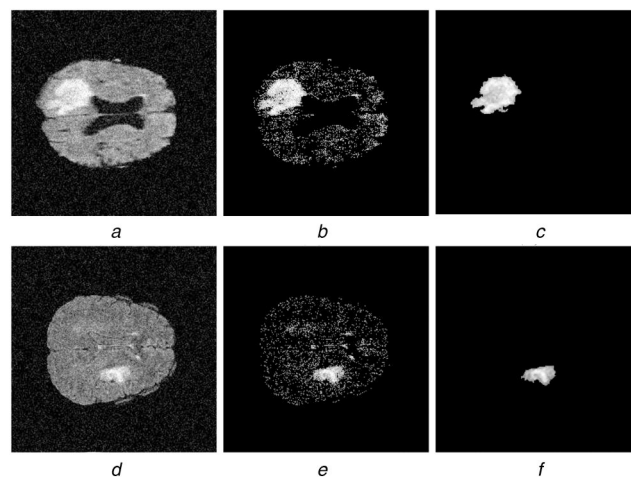


**Fig. 9** Similar results for bias field MR images  
(a), (d) Original bias field HGG and LGG MR images, (b), (e) Segmentation showing shrinkage problem, (c), (f) Segmentation by the proposed GBKS GC

**Table 1** Results obtained for 10 HGG and 10 LGG MRI images comparing the GBKS GC technique

MSE (HGG)		CC (HGG)		MSE (LGG)		CC (LGG)	
Without bias field	With bias field						
0.014	0.003	0.903	0.938	0.011	0.011	0.935	0.934
0.007	0.007	0.923	0.924	0.002	0.001	0.889	0.909
0.002	0.009	0.950	0.869	0.004	0.001	0.904	0.936
0.001	0.030	0.890	0.784	0.008	0.005	0.899	0.869
0.005	0.008	0.936	0.910	0.001	0.008	0.958	0.848
0.011	0.019	0.904	0.857	0.002	0.005	0.949	0.720
0.008	0.015	0.905	0.867	0.008	0.002	0.849	0.937
0.007	0.011	0.844	0.871	0.009	0.009	0.903	0.915
0.005	0.016	0.950	0.871	0.002	0.002	0.888	0.841
0.005	0.009	0.930	0.842	0.002	0.021	0.959	0.701

**Table 2** Average MSE and CC error for GBKS GC technique (mean±std)

	MSE		CC	
	Without bias field	With bias field	Without bias field	With bias field
HGG	0.008 ± 0.004	0.013 ± 0.001	0.899 ± 0.031	0.877 ± 0.04
LGG	0.006 ± 0.005	0.006 ± 0.005	0.919 ± 0.044	0.861 ± 0.079

comparison with the bias field images due to the presence of the noise. The result thus proves the selected kernels from the proposed technique GBKS GC are highly accurate for all the images (whether HGG or LGG) and with or without bias field which aid in the removal of shrinkage problem.

#### 4.2 Real-time dataset

The proposed GBKS GC method is applied on some real-time dataset with flair modality under the expert guidance of radiologist. Figs. 10a, c and e depict MRI brain tumour images diagnosed with meningioma, GBM and cystic acoustic schwannoma, respectively. In these figures, tumour affected portion of the brain is marked by the radiologist. The results obtained after applying the proposed technique are depicted in Figs. 10b, d and f. It is observed that the tumour regions are clearly identified and no fallacious segmentation is obtained.

These results are verified by the expert radiologist and the difficulty that occurs in having the clear vision of abnormal structures of human brain is removed by the proposed GBKS GC method.

#### 4.3 Performance metrics

The validation of the proposed GBKS GC technique is further done by evaluating the performance metrics applied on the obtained tumour region. The parameters are calculated for the ET region

with no shrinkage problem for without and with bias field MR images. It is observed from Fig. 11 that tumour is accurately extracted from the HGG MR images, with and without bias field affecting the images. Post-processing is employed on the extracted regions of the tumour to achieve the segmented glioma portion. Similarly, Fig. 12 depicts the results obtained for the LGG images. From these results, it is clear enough that the proposed algorithm successfully executes the segmentation in the presence or the absence of bias field effect.

In Tables 3 and 4, a qualitative analysis is provided for 20 HGG and 20 LGG MRI images (with and without bias effect images). All the values obtained confirm the accuracy of the segmented results. All the parameters are evaluated on scale of 0-1, values closer to 1 are perceived as good segmentation and the opposite is true for poor segmentation. The values depicted in Tables 3 and 4 for JI, DSC, PPV, sensitivity and specificity are high for images with and without bias field emphasising better segmentation. Higher DSC value represents dice overlap and from Tables 3 and 4, it is observed that the values obtain higher value inferring high similarity with the GT.

Observing the PPV value from Tables 3 and 4, low fallacious segmentation is achieved by the proposed algorithm. Also, a high sensitivity value is observed from these tables which correspond to all positives in the original image are correctly detected. Same is true for specificity parameter, where all the negatives of the original pixels are also correctly detected.

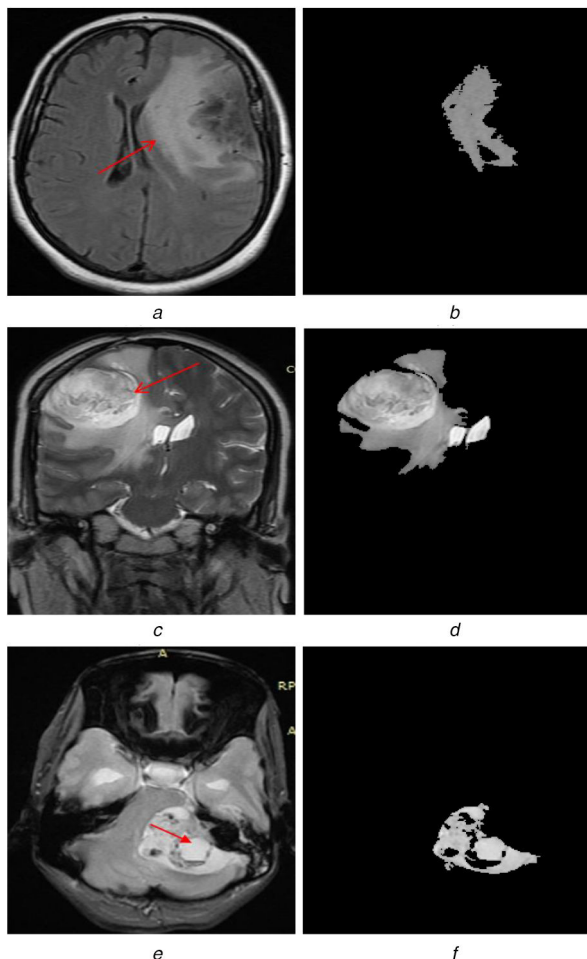


**Fig. 10** Real-time dataset

(a), (c), (e) Axial (flair) MR image diagnosed as meningioma, GBM and cystic acoustic schwannoma, (b), (d), (f) Segmented tumour region obtained by the proposed GBKS GC method

#### 4.4 Regional parameter validation

For validating the obtained tumour region from the proposed technique, regional properties of the segmented tumour are calculated as described in Section 3.5. Same regional properties are calculated for the mask of the GT of corresponding images. To validate the accuracy of ET region, the mean error for these properties is calculated and tabulated in Table 5.

To generalise the error obtained, the mean values for all the HGG and LGG images are calculated. It is observed that the mean errors obtained for HGG and LGG images are 0.11 and 0.02 for area, 0.10 and 0.01 for perimeter, 0.04 and 0.02 for maximum axis length and 0.05 and 0.05 for minimum area length, respectively.

The tabulated results signify high perimeter error for both the images, as edges formed in the output image are not smooth, whereas the boundary edges of the GT are smoother. The MAL and the MiAL infer the shape of the tumour. The result obtained by the proposed technique show occurrence of small error, hence conserving and validating the accuracy of the obtained tumour shape.

#### 4.5 Comparison to existing techniques

The average value calculated for complete dataset used for the simulation is illustrated in Table 6. The values obtained for the evaluated parameters present good result for accurate and better performance of the proposed GBKS GC technique. These results are also compared with some of the existing GC technique. The comparison is shown in Table 7. Jiang *et al.* [29] constructed a graph with the help of a priori information that is obtained from the feature sets of the multimodal magnetic resonance of population and patient specific. Although the segmentation is done by using

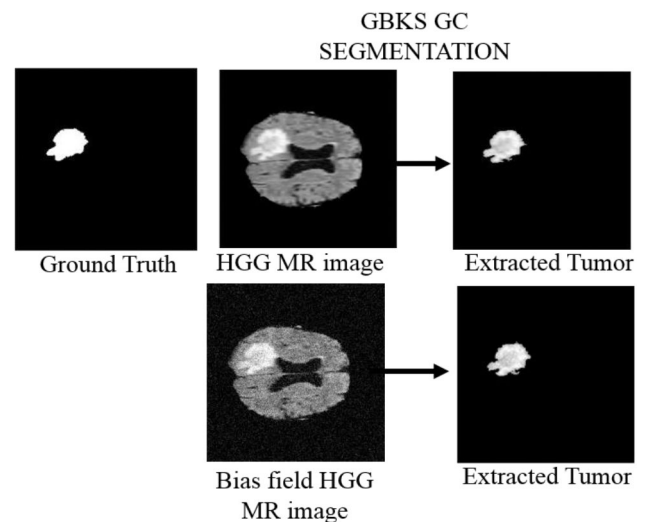


**Fig. 11** Extraction of tumour region by the proposed GBKS GC segmentation technique on brain HGG MR images with and without bias field effect

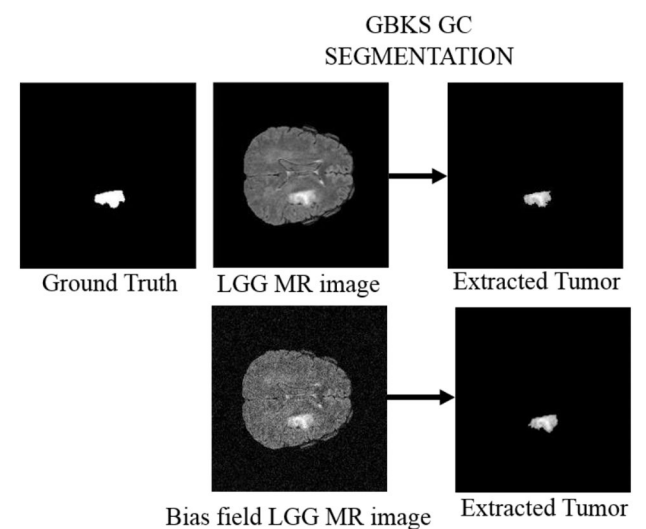


**Fig. 12** Extraction of tumour by the proposed GBKS GC segmentation technique applied on brain LGG MR images with and without bias field effect

GC technique, the seeds are manually selected. Hence, this method involves user interaction compelling it to be prone to human error. A comparison of the proposed technique with the conventional GC method [45] and random walk technique [46] is also provided in Table 7. The a priori information of the feature set is unknown in GC technique, and this information is important as this technique is intensity dependent. Also, decisions in random walk technique are based on the information derived from the pixel intensity as they form the probability distribution of the image graph. Besides, both these techniques comprise human interactions for providing the initial a priori information. These technique pose difficulties in case of shrinkage problem as the parameter values obtained are low. The comparative results are also shown graphically in Fig. 13.

## 5 Conclusion

The proposed GBKS GC method removes the hurdles involved in the interactive GC technique. The automatic selection of the proposed method eliminates the interactive nature and selected markers provide the most effective and accurate segmentation of the tumour region. This research work has addressed the open research challenge of the shrinkage problem. Even for images that have intensity inhomogeneity due to the bias field, the proposed method is successfully able to extract the targeted tumour region.

**Table 3** Evaluation results of GBKS GC method for HGG MR images (without and with bias field effect)

	Jl	DSC	PPV	Sensitivity	Specificity
HGG	0.91	0.83	0.83	0.99	0.99
	0.93	0.86	0.92	0.99	0.93
	0.95	0.91	0.98	0.99	0.91
	0.89	0.80	0.86	0.99	0.92
	0.94	0.88	0.93	0.95	0.94
	0.91	0.83	0.85	0.94	0.97
	0.91	0.83	0.83	0.89	0.99
	0.84	0.72	0.73	0.91	0.97
	0.95	0.91	0.99	0.92	0.91
	0.90	0.82	0.96	0.91	0.85
HGG with bias field	0.94	0.89	0.98	0.99	0.90
	0.93	0.86	0.89	0.99	0.97
	0.87	0.77	0.97	0.99	0.78
	0.78	0.64	0.64	0.99	0.99
	0.91	0.84	0.94	0.95	0.88
	0.87	0.76	0.81	0.94	0.93
	0.87	0.77	0.81	0.99	0.95
	0.87	0.77	0.77	0.91	0.99
	0.88	0.78	0.88	0.92	0.88
	0.92	0.84	0.86	0.91	0.84

**Table 4** Evaluation results of GBKS GC method for LGG MR images (without and with bias field effect)

	Jl	DSC	PPV	Sensitivity	Specificity
LGG	0.88	0.94	0.92	0.98	0.91
	0.89	0.79	0.93	0.99	0.85
	0.82	0.89	0.94	0.99	0.87
	0.88	0.94	0.94	0.99	0.99
	0.95	0.92	0.95	0.99	0.95
	0.95	0.91	0.95	0.99	0.95
	0.84	0.91	0.91	0.98	0.95
	0.89	0.94	0.95	0.95	0.98
	0.87	0.93	0.87	0.96	0.99
	0.93	0.96	0.95	0.98	0.97
LGG with bias field	0.94	0.88	0.91	0.99	0.98
	0.90	0.83	0.88	0.99	0.94
	0.94	0.88	0.91	0.99	0.96
	0.86	0.76	0.76	0.99	0.99
	0.85	0.74	0.77	0.99	0.95
	0.69	0.52	0.52	0.99	0.99
	0.94	0.88	0.91	0.98	0.99
	0.92	0.85	0.94	0.97	0.98
	0.83	0.71	0.71	0.96	0.99
	0.67	0.51	0.98	0.98	0.97

**Table 5** Error calculation for validation of tumour shape obtained from the GBKS GC method for ten HGG and ten LGG MR images

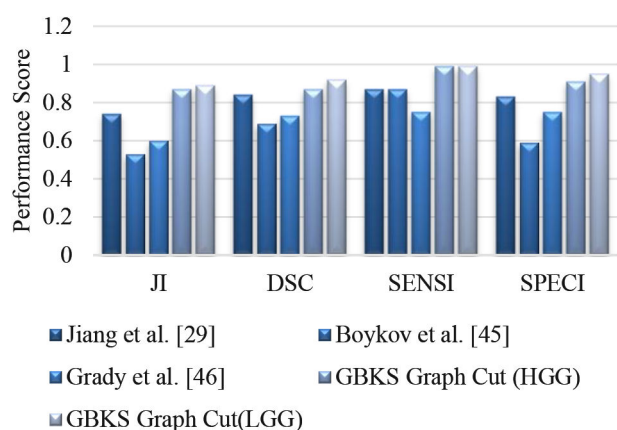
HGG				LGG			
Area	Perimeter	MAL	MiAL	Area	Perimeter	MAL	MiAL
0.11	0.06	0.01	0.05	0.01	0.08	0.10	0.05
0.17	0.17	0.06	0.01	0.01	0.06	0.07	0.11
0.06	0.03	0.02	0.05	0.07	0.03	0.05	0.09
0.12	0.01	0.01	0.13	0.01	0.02	0.07	0.05
0.11	0.06	0.13	0.04	0.01	0.01	0.04	0.05
0.02	0.03	0.06	0.09	0.01	0.06	0.03	0.06
0.03	0.08	0.12	0.14	0.11	0.04	0.03	0.12
0.05	0.15	0.08	0.04	0.01	0.02	0.05	0.06
0.16	0.05	0.01	0.14	0.01	0.08	0.01	0.08
0.02	0.02	0.02	0.01	0.02	0.09	0.02	0.01

**Table 6** Mean performance score of GBKS GC method for HGG and LGG (mean±std)

	JI	DSC	PPV	Sensitivity	Specificity
HGG	0.87 ± 0.06	0.87 ± 0.06	0.89 ± 0.07	0.99 ± 0.03	0.91 ± 0.05
LGG	0.89 ± 0.05	0.92 ± 0.04	0.93 ± 0.03	0.99 ± 0.03	0.95 ± 0.04
HGG (bias field)	0.88 ± 0.04	0.78 ± 0.07	0.86 ± 0.09	0.99 ± 0.01	0.91 ± 0.06
LGG (bias field)	0.85 ± 0.09	0.75 ± 0.13	0.83 ± 0.13	0.99 ± 0.01	0.91 ± 0.13

**Table 7** Comparison of performance metric with the existing techniques (mean±std)

	DSC	JI	Sensitivity	Specificity	PPV
Jiang <i>et al.</i> [29]	0.84 ± 0.09	0.74 ± 0.14	0.87 ± 0.07	0.83 ± 0.14	0.74 ± 0.14
Boykov and Funka-Lea [45]	0.69 ± 0.12	0.53 ± 0.15	0.87 ± 0.09	0.59 ± 0.20	0.69 ± 0.12
Grady <i>et al.</i> [46]	0.73 ± 0.16	0.60 ± 0.18	0.75 ± 0.26	0.75 ± 0.07	0.60 ± 0.18
HGG (GBKS)	0.87 ± 0.06	0.87 ± 0.06	0.99 ± 0.03	0.91 ± 0.05	0.87 ± 0.06
LGG (GBKS)	0.92 ± 0.04	0.89 ± 0.05	0.99 ± 0.03	0.95 ± 0.04	0.89 ± 0.05

**Fig. 13** Graphical representation of comparative results

The algorithm was validated by its application on the real-time dataset of different brain tumours. The brain tumour segmentation is a powerful ubiquitous clinical diagnostic tool, for detection and diagnosis of normal and pathological tissue as abnormalities and tumours. The removal of fallacious segmentation finds its application even in neurological and psychiatric disorder.

For confirming the obtained shape of the segmented tumour, the evaluated error for all the regional properties is very low. Even the shrinkage problem that produces erroneous region in the surrounding region is completely removed, and the evaluated MSE and CC values provide this validation. The JI, DSC, PPV, sensitivity and specificity performance metrics are calculated for MR images with and without bias effect. The evaluated results infer that a significant outperformance is observed for the proposed technique in comparison with all the existing techniques.

In the future, we will perform multi-segmentation within the tumour region through classification by employing neural network and artificial intelligence.

## 6 Acknowledgments

We gratefully thank the radiology department of the Indra Gandhi Medical Hospital (IGMC), Shimla, Himachal Pradesh, India, for their assistance in providing us the real-time database. We have benefitted from the expert guidance offered by the radiologist in validating the obtained results.

## 7 References

- [1] Bauer, S., Wiest, R., Nolte, L.-P., *et al.*: 'A survey of MRI-based medical image analysis for brain tumor studies', *Phys. Med. Biol.*, 2013, **58**, p. R97
- [2] Despotović, I., Goossens, B., Philips, W.: 'MRI segmentation of the human brain: challenges, methods, and applications', *Comput. Math. Meth. Med.*, 2015, **2015**, (450341), p. 23
- [3] Hanaoka, S., Fritscher, K., Welk, M., *et al.*: '3D graph cut segmentation with Riemannian metrics to avoid the shrinking problem'. Proc. Int. Conf. Medical Image Computing and Computer-Assisted Intervention, Berlin, Germany, 2011, pp. 554–561

- [4] Madabhushi, A., Metaxas, D.: 'Automatic boundary extraction of ultrasonic breast lesions'. Proc. Int. Conf. Biomedical Imaging, Washington DC, USA, 2002, pp. 601–604
- [5] Shan, J., Cheng, H.-D., Wang, Y.: 'A novel automatic seed point selection algorithm for breast ultrasound images'. Proc. Int. Conf. Pattern Recognition, Tampa, USA, 2008, pp. 1–4
- [6] Shan, J., Cheng, H., Wang, Y.: 'Completely automated segmentation approach for breast ultrasound images using multiple-domain features', *Ultrasound Med. Biol.*, 2012, **38**, pp. 262–275
- [7] Chen, X., Pan, L.: 'A survey of graph cuts/graph search based medical image segmentation', *IEEE Rev. Biomed. Eng.*, 2018, **11**, pp. 112–124
- [8] Le, T.H., Jung, S.W., Choi, K.S., *et al.*: 'Image segmentation based on modified graph-cut algorithm', *Electron. Lett.*, 2010, **46**, (16), pp. 1121–1123
- [9] Boykov, Y.Y., Jolly, M.-P.: 'Interactive graph cuts for optimal boundary & region segmentation of objects in ND images'. Proc. Int. Conf. Computer Vision, Vancouver, Canada, 2001, pp. 105–111
- [10] Rother, C., Kolmogorov, V., Blake, A.: 'GrabCut: interactive foreground extraction using iterated graph cuts', *ACM Trans. Graph.*, 2004, **23**, pp. 309–314
- [11] Mortensen, E.N., Barrett, W.A.: 'Intelligent scissors for image composition'. Proc. Int. Conf. Computer Graphics and Interactive Techniques, New York, NY, USA, 1995, pp. 191–198
- [12] Jermyn, I.H., Ishikawa, H.: 'Globally optimal regions and boundaries as minimum ratio weight cycles', *IEEE Trans. Pattern Anal. Mach. Intell.*, 2001, **23**, pp. 1075–1088
- [13] Sinop, A.K., Grady, L.: 'A seeded image segmentation framework unifying graph cuts and random walker which yields a new algorithm'. Proc. Int. Conf. Computer Vision, Rio de Janeiro, Brazil, 2007, pp. 1–8
- [14] Kimmel, R., Bruckstein, A.M.: 'Regularized Laplacian zero crossings as optimal edge integrators', *Int. J. Comput. Vis.*, 2003, **53**, pp. 225–243
- [15] Kolmogorov, V., Boykov, Y.: 'What metrics can be approximated by geo-cuts, or global optimization of length/area and flux'. Proc. Int. Conf. Computer Vision, Beijing, China, 2005, pp. 564–571
- [16] Boykov, Y., Veksler, O., Zabih, R.: 'Fast approximate energy minimization via graph cuts', *IEEE Trans. Pattern Anal. Mach. Intell.*, 2001, **23**, pp. 1222–1239
- [17] Shi, J., Malik, J.: 'Normalized cuts and image segmentation', *IEEE Trans. Pattern Anal. Mach. Intell.*, 2000, **22**, pp. 888–905
- [18] Hao, Z., Wang, Q., Ren, H., *et al.*: 'Multiscale superpixel classification for tumor segmentation in breast ultrasound images'. Proc. Int. Conf. Image Processing (ICIP), Orlando, USA, 2012, pp. 2817–2820
- [19] Gao, L., Yang, W., Liao, Z., *et al.*: 'Segmentation of ultrasonic breast tumors based on homogeneous patch', *Med. Phys.*, 2012, **39**, pp. 3299–3318
- [20] Alemán-Flores, M., Álvarez, L., Caselles, V.: 'Texture-oriented anisotropic filtering and geodesic active contours in breast tumor ultrasound segmentation', *J. Math. Imaging Vis.*, 2007, **28**, pp. 81–97
- [21] Liu, X., Huo, Z., Zhang, J.: 'Automated segmentation of breast lesions in ultrasound images'. Proc. Int. Conf. Engineering in Medicine and Biology Society IEEE-EMBS, Shanghai, China, 2006, pp. 7433–7435
- [22] Sled, J.G., Zijdenbos, A.P., Evans, A.C.: 'A nonparametric method for automatic correction of intensity non-uniformity in MRI data', *IEEE Trans. Med. Imaging*, 1998, **17**, (1), pp. 87–97
- [23] Wells, W.M., Crimson, W.E.L., Kikinis, R., *et al.*: 'Adaptive segmentation of MRI data', *IEEE Trans. Med. Imaging*, 1996, **15**, (4), pp. 429–442
- [24] Li, C., Xu, C., Anderson, A., *et al.*: 'MRI tissue classification and bias field estimation based on coherent local intensity clustering: a unified energy minimization framework'. Proc. Int. Conf. Information Processing in Medical Imaging, Williamsburg, VA, USA, July 2009, pp. 289–299
- [25] Bilenia, A., Sharma, D., Raj, H., *et al.*: 'Brain tumor segmentation with skull stripping and modified fuzzy C-means'. Information and Communication Technology for Intelligent System, Singapore, 2019, pp. 229–237
- [26] Szwarc, P., Kawa, J., Rudzki, M., *et al.*: 'Automatic brain tumour detection and neovascularity assessment with multiseries MRI analysis', *Comput. Med. Imaging Graph.*, 2015, **46**, pp. 178–190
- [27] Popuri, K., Cobzas, D., Murtha, A., *et al.*: '3D variational brain tumor segmentation using Dirichlet priors on a clustered feature set', *Int. J. Comput. Assist. Radiol. Surg.*, 2012, **7**, pp. 493–506

- [28] Kanas, V.G., Zacharaki, E.I., Davatzikos, C., *et al.*: 'A low cost approach for brain tumor segmentation based on intensity modeling and 3D random walker', *Biomed. Signal Proc. Control*, 2015, **22**, pp. 19–30
- [29] Jiang, J., Wu, Y., Huang, M., *et al.*: '3D brain tumor segmentation in multimodal MR images based on learning population- and patient-specific feature sets', *Comput. Med. Imaging Graph.*, 2013, **37**, pp. 512–521
- [30] Zhao, L., Sarikaya, D., Corso, J.J.: 'Automatic brain tumor segmentation with MRF on supervoxels', *Multimodal Brain Tumor Segmentation*, 2013, **51**
- [31] Ilunga-Mbuyamba, E., Avina-Cervantes, J.G., Garcia-Perez, A., *et al.*: 'Localized active contour model with background intensity compensation applied on automatic MR brain tumor segmentation', *Neurocomputing*, 2017, **220**, pp. 84–97
- [32] Havaei, M., Davy, A., Warde-Farley, D., *et al.*: 'Brain tumor segmentation with deep neural networks', *Med. Image Anal.*, 2017, **35**, pp. 18–31
- [33] Kleesiek, J., Biller, A., Urban, G., *et al.*: 'Ilastik for multi-modal brain tumor segmentation', Proc. Int. Conf. MICCAI BRATS (Brain Tumor Segmentation Challenge), Boston, USA, 2014, pp. 12–17
- [34] Zikic, D., Ioannou, Y., Brown, M., *et al.*: 'Segmentation of brain tumor tissues with convolutional neural networks', Proc. Int. Conf. MICCAI-BRATS, Boston, USA, 2014, pp. 36–39
- [35] Havaei, M., Larochelle, H., Poulin, P., *et al.*: 'Within-brain classification for brain tumor segmentation', *Int. J. Comput. Assist. Radiol. Surg.*, 2016, **11**, pp. 777–788
- [36] Li, Y., Jia, F., Qin, J.: 'Brain tumor segmentation from multimodal magnetic resonance images via sparse representation', *Artif. Intell. Med.*, 2016, **73**, pp. 1–13
- [37] Wu, K., Yizhou, Y.: 'Automatic object extraction from images using deep neural networks and the level-set method', *IET Image Process.*, 2018, **12**, (7), pp. 1131–1141
- [38] Bakas, S., Akbari, H., Sotiras, A., *et al.*: 'Advancing the cancer genome atlas glioma MRI collections with expert segmentation labels and radiomic features', *Sci. Data*, 2017, **4**, p.170117
- [39] Menze, B.H., Jakab, A., Bauer, S., *et al.*: 'The multimodal brain tumor image segmentation benchmark (BRATS)', *IEEE Trans. Med. Imaging*, 2015, **34**, pp. 1993–2024
- [40] Menze, B.H., Van Leemput, K., Lashkari, D., *et al.*: 'A generative model for brain tumor segmentation in multi-modal images', Proc. Int. Conf. Medical Image Computing and Computer-Assisted Intervention, Berlin, Germany, 2010, pp. 151–159
- [41] Rao, B.D., Goswami, M.M.: 'A comprehensive study of features used for brain tumor detection and segmentation from MR images', Innovations in Power and Advanced Computing Technologies (i-PACT), Vellore, India, 2017, pp. 1–6
- [42] Rosenfeld, A., Pfaltz, J.L.: 'Sequential operations in digital picture processing', *J. ACM*, 1966, **13**, pp. 471–494
- [43] Park, C., Huang, J.Z., Ji, J.X., *et al.*: 'Segmentation, inference and classification of partially overlapping nanoparticles', *IEEE Trans. Pattern Anal. Mach. Intell.*, 2013, **35**, p. 1
- [44] Dogra, J., Jain, S., Sood, M.: 'Segmentation of MR images using hybrid *k* mean-graph cut technique', *Procedia Comput. Sci.*, 2018, **132**, pp. 775–784
- [45] Boykov, Y., Funka-Lea, G.: 'Graph cuts and efficient ND image segmentation', *Int. J. Comput. Vis.*, 2006, **70**, pp. 109–131
- [46] Grady, L., Schiwietz, T., Aharon, S., *et al.*: 'Random walks for interactive organ segmentation in two and three dimensions: implementation and validation', Proc. Int. Conf. Medical Image Computing and Computer-Assisted Intervention, Berlin, Germany, 2005, pp. 773–780